Non-contact damage detection on a rotating blade by Lamb wave analysis

Veira Canle, Daniel

2017

Veira Canle , D , Salmi , A H & Haeggström , E O 2017 , ' Non-contact damage detection on a rotating blade by Lamb wave analysis ' , NDT & E International , vol. 92 , pp. 159-166 . https://doi.org/10.1016/j.ndt

http://hdl.handle.net/10138/307966
https://doi.org/10.1016/j.ndteint.2017.08.008

Non-contact damage detection on a rotating blade by Lamb wave analysis.

Daniel Veira Canle,[1,a)] Ari Salmi,[1,b)] Edward Hæggström[1,c)]

Department of Physics, University of Helsinki, Helsinki, 00560, Finland

Abstract

Propeller inspection is mandatory for safe operation of aircraft. Damage evaluation on such rotating structures requires dedicated measurement techniques. In this study efforts to create a stroboscopic technique are reported. Lamb waves were excited on a rotating blade with a Q-switched Nd:YAG laser synchronized to the sample rotation, whereas the wave amplitude was obtained by a laser Doppler vibrometer. A surface breaking notch on an aluminum sample rotating at 415 rpm was detected and sized with millimeter accuracy. The technique has potential for automatic non-contacting damage detection on rotating structures such as helicopter blades and turbines.

Keywords: Non-contacting NDE, Lamb waves, notch detection, rotating target.

I. INTRODUCTION

Propellers are key components in vehicles and machinery, such as helicopters, ships, and power plants. Technical inspection is required to ensure safe operation. According to the US Federal Aviation Administration (FAA), aircraft propeller integrity can be compromised due to e.g. delamination, corrosion, lightning strikes, stone nicks, *etc* [1] [2] [3]. Northrop Inc., under a contract from the US Air Force, set several requirements for flaw detection techniques: the inspection should be carried out with reliable sensors capable of detecting cracks, 1.25mm in length, situated in complicated locations such as sharp edges, apertures, and rivets [4]. The fact that propellers carry coatings often made of composites, make testing challenging. Ideally, one would want to quickly inspect propellers in motion since then aircraft could immediately take off after scanning. This would increase the service time of the machine and decrease inspection costs.

To achieve flaw detection that fulfils these specifications, several techniques are used but all have certain limitations. Thermal imaging [5] cannot detect small internal defects and is limited to heat conducting materials. X-rays can scan a wide range of materials of different thickness and can provide high resolution images of defects [6]. However, radiography is expensive and a sample must be extracted for analysis which makes it impossible to do in-service damage detection [7]. Eddy-current testing allows flaw detection [8], however, this inexpensive and sensitive technique is limited to surface defects in conductive samples. Ultrasonic damage evaluation is an alternative/complement to the aforementioned inspection methods. This method, often based on bulk waves or Lamb wave excitation and detection, can image both surfaces and internal defects in moving samples [9] [10].

Lamb waves are guided elastic waves that are suitable for flaw detection. These dispersive surface waves propagate in plates with free boundaries [11] [12], featuring two particle displacement components, one parallel to the surface of the plate and another one perpendicular to it. The velocity of these symmetric and antisymmetric modes is a function of the plate thickness and the sound frequency. Hence the wave modes travel at different speed when they propagate across defects compared to when they travel across unharmed parts of the plate. The

a)Corresponding author at: Departments of Physics, University of Helsinki, Helsinki, Finland. daniel.veiracanle@helsinki.fi
b) ari.salmi@helsinki.fi c) edward.haeggstrom@helsinki.fi

reason is that the damaged region is thinner than the undamaged plate. These guided waves can propagate even meters of distance and can interact with both surface and bulk defects.

Lamb wave based flaw detection is usually done with contacting transducers [4] [13] [14]. The resolution of a transducer array is limited by the distance between its sensing elements as well as by the inspection wavelength [15, 16]. Therefore, high transducer density (many transducers per area) is required to carry out experiments [4] [15] [16]. The transducers modify the dynamic properties of the propeller and wiring is cumbersome in moving blades [2] [16]. In addition, acoustic impedance matching between the transducers and the sample is nontrivial [17].

Laser ultrasonics (LU) employs a laser to excite elastic waves that often are detected optically. One illuminates the sample with a high power pulsed (100 mJ per pulse) laser beam to excite propagating ultrasonic waves and another laser, usually a laser Doppler vibrometer (LDV) detects the surface waves. LU can analyze moving samples in hazardous environments [3] [18] [17]. Furthermore, it permits fast and large area scans, and it provides high spatial resolution imaging and remote access [9] [2]. Unfortunately, LU usually features lower SNR than contacting techniques. Treatment of the sample surface may be required to maximize the amount of light collected by the read-out interferometer. One can sometimes apply a reflective coating (e.g. by spraying) and use a laser detection system with high power while keeping the laser excitation at low power to avoid damaging the sample. Using line excitation [19], an IDT-like group of lines [20], or even curves for focusing [21] can remove the need to work in the ablation regime. Any applied coating needs to be removed after inspection [22].

By means of LU, defects, such as cavities [18], cracks [2] [24], and holes [25] have been detected, sized, and imaged in plates. Imaging of delamination defects on wind turbine blades has been achieved by B.Park *et.al* [9].Ultrasonic methods such as contacting, air coupled, and immersion, transducers have also been used to determine the size of cracks [26], holes [13], bonding flaws [27][18] and delaminations [28] in plates and even to study stress accumulation in automobile break pads [29].

As far as damage detection is concerned, there are no previous studies that characterize a notch on a rotating propeller in a non-contact way. Park *et.al* successfully tested a non-contacting method to image cracks in propellers but the experiment they performed was on a static aluminium plate [2]. They also carried out experiments on a moving propeller but they embedded transducers in the sample which makes it a contacting method [3].In another article, Park *et.al* suggested and tested a laser ultrasound damage detection technique on a static wind turbine blade. Finally, in reference [13], Raišutis *et.al* imaged defects on a static wind turbine blade using air coupled transducers.

Regardless of the progress in the field of NDE of rotating propeller-like structures, there is still a need for a non-contacting *in situ* damage evaluation technique. In this study, a laser excitation, laser pickup based stroboscopic method utilizing Lamb waves is developed, enabling crack detection in a rotating propeller.

II. STROBOSCOPIC TECHNIQUES FOR DAMAGE DETECTION

To develop a stroboscopic method for Lamb wave inspection of rotating propeller-like structures, two bowtie-shaped samples (130x75.20x4 mm^3in size) made of aluminum were studied (Fig.1). One sample featured a 5x10x2.4 mm^3 surface breaking rectangular defect

situated 35.10 mm from the center. The other propeller was intact and served as a reference sample.

The setup (Fig.1) featured a CFR Big Sky Laser Series pulsed Q-switched laser (8 ns, 189 mJ, adjustable PRF (maximum 10 Hz)) for Lamb wave excitation, and a Polytec OFV303 laser Doppler Vibrometer (24 MHz bandwidth in displacement mode) for detection. The sample was rotated by a 12V DC motor to which a pulse width modulated signal was fed from a custom made circuit based on the 555 timer. The bow-tie shaped sample rotated at 415 rpm (linear velocity of its proximal edges was 2.7 ms^{-1}). The rotation was monitored by a custom made optical gate built using a blue LED, a PDB-C142 blue enhanced photodiode, and a LM311 comparator. The gate signals were sent to an Arduino Mega 2560 microcontroller. Based on the instructions sent from a computer running LabView 2012 (64 bit, National Instruments, 2012) the microcontroller decided when to fire the excitation laser.

The alignment of the LDV with respect to the sample is crucial since if the laser beam is reflected from the sample at an angle only a small fraction of the reflected light is collected by the detector. However, no error is introduced into the gathered data because the obtained dispersion curves match the theoretical ones. Therefore, proper laser alignment is necessary to have a high SNR.

Two measurements were performed: A line and an arc scheme, see Fig. 2. In the line scan (Fig 2A), to ensure that the centre of the blade was hit, an Arduino based photogate system measured the time duration that the blade shadowed the LED (time delay). The excitation laser was then triggered at one half of the time delay once every eight passes of the blade (a PRF of 1.2 Hz). The LDV was focused 9.6 mm from the centre of the sample while the excitation point was near the edge. The excitation laser scanned the sample by a mirror positioned on top of a translation stage, which was moved in steps of (0.239 ± 0.014) mm after 80 shots of the Nd:YAG at a given measurement point. Therefore, for the linear scan 80 samples were measured at 232 points evenly spaced across the length of the propeller.

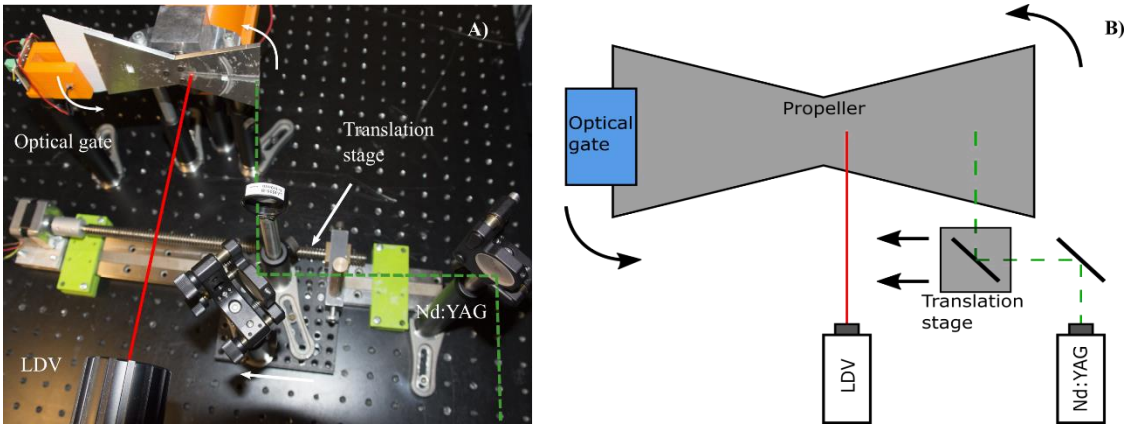

Figure 1. Measurement setup for damage detection on a rotating propeller at 415 rpm. A) Picture of the setup with the notched propeller. B) Schematics of the measurement system. The Nd:YAG laser scans the length of the sample by means of a mirror attached to a translation stage.

The second type of scan (Fig 2B) was used to study wave propagation across the width of a rotating propeller. Here the excitation and pick up points were fixed at different locations, always 32.6 mm apart. The microcontroller calculated the time that the light in the optical gate was blocked by the blade, i.e. the time between two successive edges of the propeller. Next,

the time interval was evenly divided into 200 intervals. After eight rotations and a time t has passed (Eq.1) the Nd:YAG fires at the middle point of each sector.

$$t = (i + 1/2)\, t_{delay} \quad i = 1, \ldots, 200 \tag{1}$$

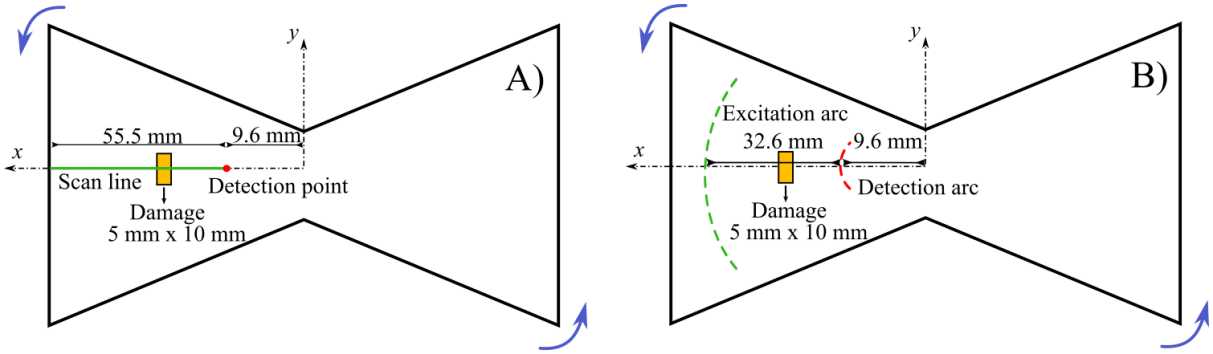

Figure 2. Representations of the scanning methods used for damage evaluation in an aluminum propeller rotating at 415 rpm. a) In a linear scan the excitation moves towards the center along the solid line (green) closing in on the pickup point (red). b) In the arc scan the Nd:YAG (green) and the LDV (red) scan paths are concentric so that the distance that the Lamb waves propagate is constant.

In Eq.1 t is the time vector that allows the synchronization between the rotation of the blade and the firing of the excitation laser, i is an integer taking values from 1 to 200 and t_{delay} the time that the propeller blocks the light beam from the LED. In the experiments one arc was measured at 1.2 Hz sampling frequency. The total number of scanning points along the arc was 200.

The fluttering motion of the sample was one of the most important factors that increased the measurement uncertainty. This kind of noise is coherent as it appears periodically during every rotational cycle (Fig.3). Thus, mean filtering is insufficient for data analysis as it only reduces incoherent noise. To tackle this problem, it was necessary to perform three experiments for both for the "linear scan" and the "arc scan". Every batch of data was median filtered to cancel out the coherent noise and finally the average of the calculated parameters was calculated.

To ensure spatial accuracy of the measurement points, the time jitter of the system (26 μs) was measured. The highest linear velocity of the blade was 2.7 ms^{-1} which corresponds to a maximum lateral deviation of 0.07 mm, which was negligible for the purposes of this study. The distance accuracy along the scan path was given by the accuracy of the translation stage which was 0.014 mm.

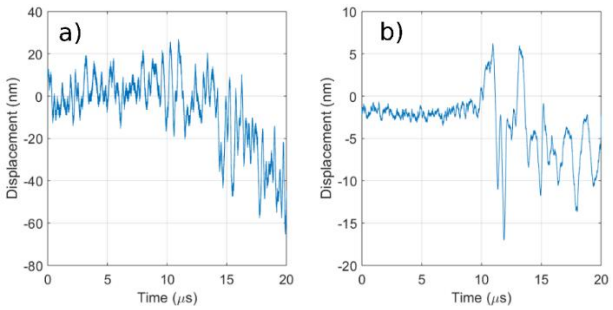

Figure 3. Signal before and after median filtering. (a) raw data where oscillations create confounding motion which prevents one from determining the Lamb wave arrival. (b) Median filtered data for a 80 experimental data points. The A_0 mode arrives at 10μs.

Unfortunately, the experiments were slow. For example, the "linear scan" took three hours. However, it could be performed faster if the pulse repetition rate is increased. The Nd:YAG laser used in this experiment can fire with a maximum PRF of 10 Hz which means that the experiment could be done in 18 minutes. It was necessary to perform the experiments at low PRF because the higher the repetition frequency of the Nd:YAG laser the smaller the amount of energy per pulse and thus the lower the signal-to-noise ratio. It has been observed experimentally that it takes Lamb waves 120 μs to dissipate. If a system is devised that fires every 120 μs (8.3 kHz PRF) the scan would be completed in 2.4 seconds. In the described experiments the axial resolution was at best 1.5 mm at 2 MHz while the lateral resolution was determined by the mesh grid of the arc scan, in this case 0.16 mm. A way to speed up the experiment is by increasing the stepping distance or the number of Nd:YAG lasers [32].

The A_0 mode group velocity was determined by fitting, in least squares sense, a line to the experimental data from the A_0 first arrival. The time of arrival of the A_0 wave front was obtained manually from the data plot. The arrival of the A_0 mode is different than that of the symmetric mode since the S_0 mode is faster than the antisymmetric Lamb wave thus arriving earlier. In addition, the LDV is more sensitive to the A_0 mode because the wave amplitude is much larger than in the case of the S_0 mode.

Furthermore, the distance from the notch to the center of the blade is given by the group velocity times the time-of-arrival of the first reflected wavefront. To determine the distance from the notch to the center of the propeller the distance between the LDV pickup point and the center (9.6 mm) was added to the calculated value.

III. RAY TRACING MODEL FOR LAMB WAVE PROPAGATION

In the proposed theoretical model, it is assumed that the Lamb waves propagate like plane waves, i.e that ray theory is applicable to explain wave propagation while ignoring absorption, attenuation, and scattering. Furthermore, the defect is considered to be perpendicular to the surface of the sample, and is considered to feature sharp corners (Fig.4).

Given two points that lie outside of and at both sides of a rectangular notch (Fig.4) the distance travelled inside the defect R is:

$$R = \begin{cases} h & \text{if } \beta < \alpha < \gamma \\ a/\cos\alpha & \text{if } 0 < \alpha < \beta \end{cases} \quad (2)$$

$$h = \sqrt{(a - (v - b/2)/\tan\alpha)^2 + (b/2 - (u - a)\tan\alpha)^2} \quad (3)$$

In Eq. 2, h is the distance that the wave travels inside the notch when the angle α (see Fig.4) is between β and γ. Here β and γ are the values that the angle α takes between the upper corners of the notch, a is the length of the notch (5 mm) and b is its width (10 mm). u and v are the projections along the x and the y axis for a Lamb wave that travels following a path at an angle α between β and γ. Equation 3 was derived for a coordinate system set at the center of the sample. Since the notch is a rectangle Eq.3 can also be applied to the lower half of the notch since the defect is symmetrical. The distance between the excitation and pick up point is d. In a pitch-catch experiment there are certain points for which the waves propagate across the notch.

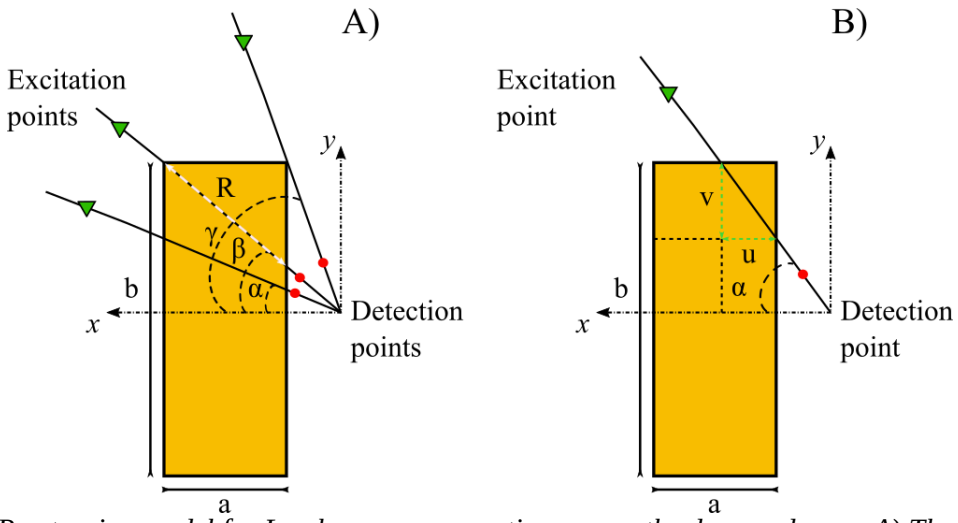

Figure 4. Ray tracing model for Lamb wave propagation across the damaged area. A) The LDV (red) and Nd:YAG (green) lie on the same line. Here, x and y denote the coordinate axes, a and b the length and width of the notch and R the distance that the sound travels inside the defect. β and γ are the angles at which the sound path meets the upper left corner and the upper right corner of the notch, respectively, whereas α is an arbitrary angle. B) Propagation of sound across the upper half of the notch. Here u and v are the projections of the sound path along the x and y axis respectively.

$$d = d_1 + R \tag{4}$$

$$t = t_1 + t_2 \tag{5}$$

Here d_1 is the distance travelled outside the notch; t_1 and t_2 are the times that the wave propagates inside and outside the defect, respectively. Equation 5 is related to the wave's group velocity leading to the equation for the time of flight

$$t = (d - R)/v_1 + R/v_2 \tag{6}$$

where v_1 and v_2 are the wave velocities outside and inside the notch respectively.

IV. ALGORITHM FOR DATA ANALYSIS

When a propeller that features a pit is sampled in an arc scan experiment, Lamb waves propagate through the damaged area. As a result, the antisymmetric mode A_0 slows down according to the theoretical dispersion curves [12].

Since the distance from the excitation point to the data pickup point is constant for the arc scan the dependence of the time-of-flight on the distance is uniform across the examined area. However, if there is a defect such as a notch in the scanned sector, a fraction of the propagating wave front is delayed, which will be apparent in the image (See Fig.7).

Software was used to identify the size of the defect (Matlab R2016a). The curvature of the antisymmetric wave front was predicted with a ray tracing model which provides an estimate of the width of the notch. To make the notch identification easier, the data were *post hoc* digitally filtered using an infinite impulse response 4th order Butterworth high-pass filter. The sampling frequency of the filter was adjusted to that of the oscilloscope, 1 GHz, the stopband frequency was 0.1 MHz, and the passband frequency was 2 MHz.

Once the damaged area was identified, a Matlab function compared every point of the data matrix to its surrounding neighbors. If the color intensity of such a point was within the threshold introduced by the user the point was extracted for further analysis. For this study, the threshold was estimated by visual inspection of the color scale of both the damaged and undamaged regions.

V. RESULTS

The calculations of the uncertainties that correspond to the calculated parameters are presented in Appendix B.

In the linear scan (Fig.5) the distance corresponds to the x axis in Fig.2. As seen from the figure, both the S_0 mode and the antisymmetric modes propagate at a measured group velocity of $(4370 \pm 60)\ \mathrm{ms}^{-1}$and $v_g = (3180 \pm 32)\ \mathrm{ms}^{-1}$, respectively. The arrival of the A_0 mode has been highlighted with a thick red dashed line. The faster S_0 mode arrives earlier to the detection spot and it is seen as lines of different slope in the upper right hand corner of the graph. Besides these two modes, there were multiple higher order modes (Fig.6) but their contribution to the particle displacement was negligible.

The notch length *a* is estimated from the time difference between two successive reflections of the A_0 mode. These reflections are the perpendicular lines orthogonal to the main antisymmetric mode wave front in Fig.5 (marked with black arrows). The obtained notch length is $a = (5.7 \pm 1.8)\ \mathrm{mm}$. From the group velocity of the A_0 mode and the time-of-flight of the reflected wave front one can compute the distance from the center of the blade to the notch namely $d = (34.6 \pm 2.2)\ \mathrm{mm}$.

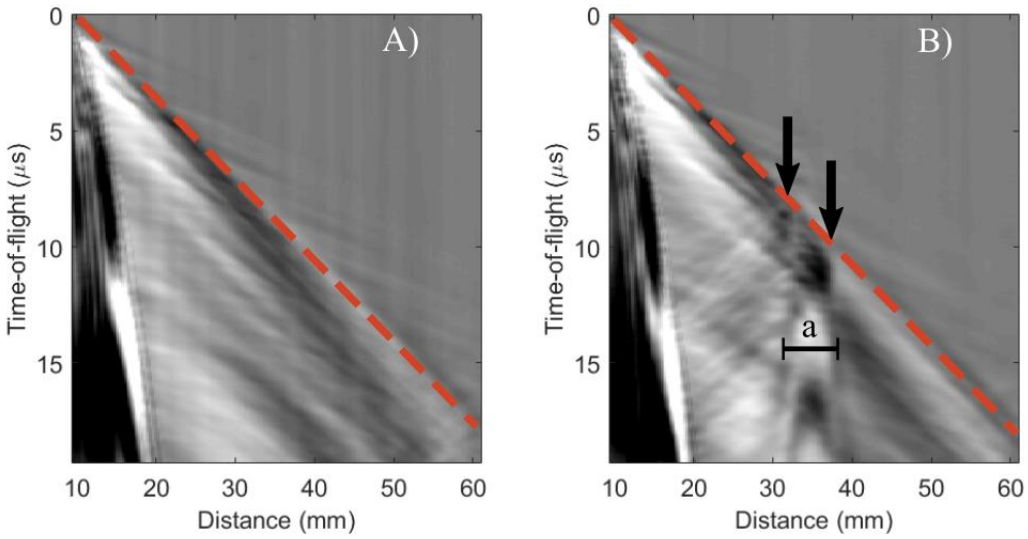

Figure 5. Linear scan of the rotating reference (a) and notched propellers (b) at 415 rpm. The red line represents the linear fit from which the A_0 group velocity is calculated. The first and second reflections at the boundaries of the notch are marked with arrows (black). Their positions were determined by visual inspection of the figure, and by manually selecting the points where the reflected wave fronts intersected with the arriving A_0 wave front. The vertical lines on the left-hand side represent the shock wave front travelling at Mach 2.2 that was caused by laser ablation and that was detected by the LDV. In addition, there are vertical lines across the figures arising from background noise.

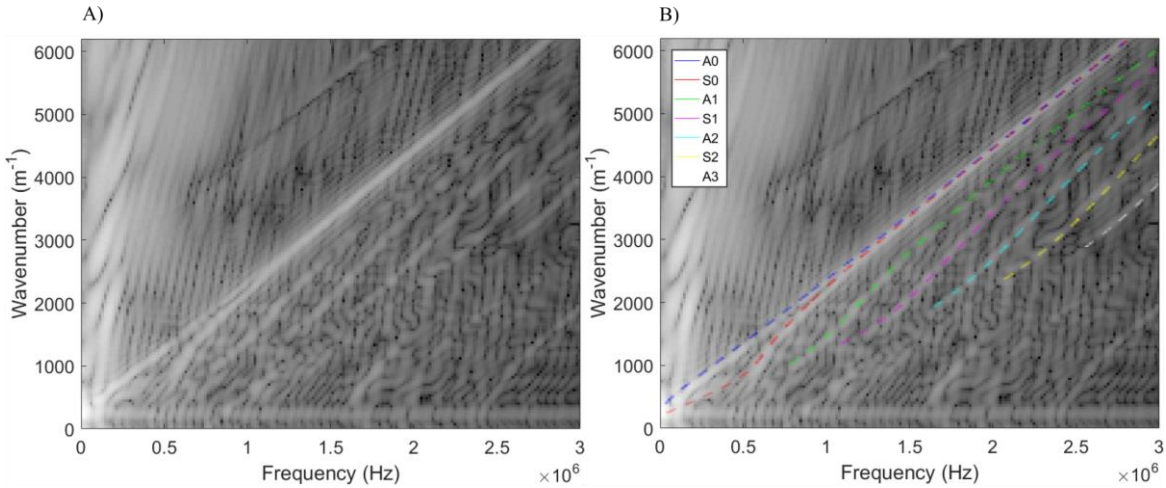

Figure 6. 2D-FFT of rotating reference sample. A) Shape of the dispersion curves obtained experimentally. B) They did not change due to sample rotation compared to when it was at rest, i.e. the stroboscopic measurement was stable (the time stepping worked correctly). The experimentally determined mode shapes did not differ from the theoretically predicted mode shapes (colored lines). The propagating Lamb wave modes range from $\mathbf{A_0}$ *up to* $\mathbf{A_3}$.

Analyzing Fig.7 one can estimate the width of the notch, *b*, by considering the distance interval (corresponding to the y axis of Fig.2) where the A_0 mode is retarded. This is a curved A_0 wave front yielding a result $b = (9.30 \pm 0.92)$ mm.

Solving Eq.6 for v_2 yields a phase velocity:

$$v_2 = R[t - (d - R)/v_1]^{-1} \quad (7)$$

Leading to $v_2 = (1686 \pm 371)\ ms^{-1}$. From the dispersion curves [11, 12] for a 4 mm thick aluminum plate one can calculate the center frequency of the fastest A_0 mode for the group velocity inside the notch $f = (2.09 \pm 0.24)\ 10^5$ Hz .

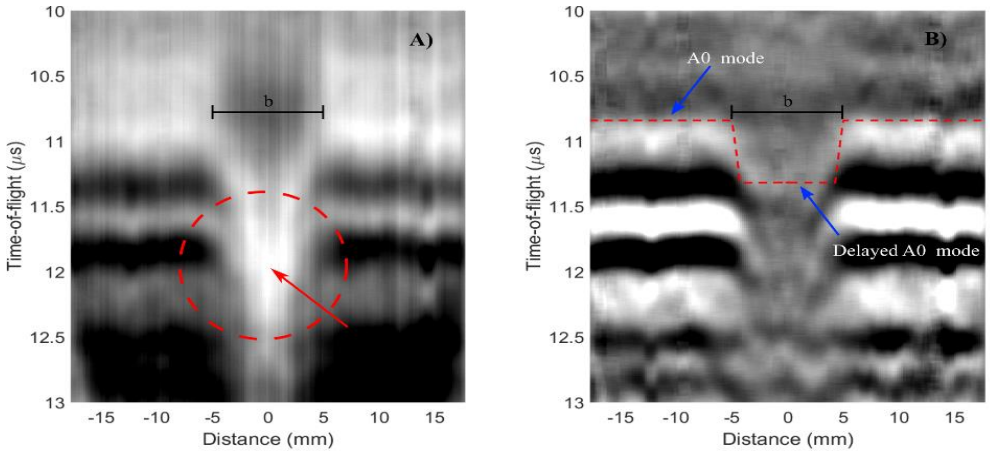

Figure 7. Stroboscopic arc scan of damaged propeller rotating at 415 rpm. a) The effect of the notch on the group velocity that was visible in figure 5 appears as a retarded $\boldsymbol{A_0}$ *front. The arrow indicates the midpoint of the distorted* $\mathbf{A_0}$ *front. b) High pass filtered waterfall plot. The experimental data agrees with the equations used to describe Lamb wave propagation (Eq 2 to 6). The theoretical shape of the antisymmetric wave front is depicted as a red dashed line.*

The theoretical approach (Eq.2 to Eq.6) was tested by high pass filtering the measurement data (Fig.7). Despite of its simplicity, it predicts the shape of the A_0 wave front that has travelled across the rectangular pit on the propeller blade.

From v_2 one can compute the frequency times thickness product (refer to Appendix A) and directly calculate the depth of the notch $D = (2.3 \pm 1.0)$ mm. These two scans, the arc scan and the linear scan allowed the calculation of the position and dimensions of the damaged area (Table 1).

TABLE I: Comparison between real notch dimensions and calculated values.

	Estimated value (mm)	Real value (mm)
Length (a)	5.7 ± 1.8	5
Width (b)	9.30 ± 0.92	10
Depth (D)	2.3 ± 1.0	2.4
Distance (d)	34.6 ± 2.2	35.1

V. DISCUSSION

A stroboscopic scanning method was developed to inspect rotating structures in a non-contacting way. The results show that this technique is valid as it is possible to detect damage and since the mode structure did not change as a result of jitter in the stroboscopic measurements.

The experiments reveal the position and size of a surface breaking rectangular flaw (Table 1). The data identify a defect in a rotating propeller. Therefore, the techniques could allow in-service damage evaluation of rotating blades without the need to stop the structure to be studied.

The experimental data supports the choice of the ray tracing model that was used to predict the effect of the notch on the A_0 wave front (Fig.7). However, this approximation is crude as it assumes that Lamb waves travel in straight lines like ideal plane waves. The model imperfectly matches at the corners of the notch because they are not sharp: their radius is 0.5 mm, which is ignored in the model Eq. 2-6. Furthermore, this theoretical model is limited to rectangular notches. If one would want to study circular defects one would have to reformulate the problem and calculate the sound path inside the flaw taking into account the circular geometry. For arbitrary shapes a standing wave filter could be used instead of a ray tracing model as suggested by Park *et.al* [3].

The pulsed laser generated broad band Lamb waves that are seen in Fig.5. The S_0 mode appears as lines of different slope than the A_0 mode since the symmetric mode propagates at a higher group velocity than the antisymmetric one. These wave modes quickly dispersed leading to wave fronts that were not particularly steep at their leading edge. As a result, it was necessary to manually pick the values for the time-of-flight of the A_0 arrival. The hypothesis was that the time of flight of the mid point of the wave front corresponded to the average time of arrival of the A_0 mode. The images obtained from raw data (Fig.5,7) are therefore a superposition of waves of many frequencies. High frequency components are interesting because they have a short wavelength, and consequently, can probe smaller defects without scattering becoming important. As a matter of fact, for the A_0 mode at 2 MHz $\lambda = 1.5$ mm and the features of the notch, e.g. corners, appear clearly in the image (Fig.7). However, high-pass filtering the data was not possible since filtering removes the reflected wave fronts from Fig.7 which makes it impossible to determine the notch size. To facilitate defect detection, one could use Lamb

waves with a specific frequency and shape. This can be done by modulating the exciting signal spatially and/or temporally [33, 34].

When a laser pulse is emitted from the Nd:YAG laser and illuminates the sample some of the sample surface material is ejected and a plasma plume is formed. Because of this energetic event, a shockwave propagating through air is created. This shockwave induces a change in the refractive index of the air through which the LDV laser beam travels and it appears as an artifact on the left-hand side of figure 5.

The measurements were performed in the ablation regime to increase the SNR since the fluttering motion of the propeller severely decreased the SNR. The main drawback is that in this regime part of the material is ejected from the surface because the laser pulse energy is so large that it evaporates the region that illuminates.

The depth of the craters created by ablation is in the range of tens of micrometers [35] and this probably doesn't affect the structural integrity of the propeller. These small induced defects might theoretically act as crack initiators in the long term and a thorough analysis should be considered.

Despite of the limitations of the technique, when compared to conventional damage detection methods, it allows true non-contact structural health monitoring of rotating structures. Finally, the algorithms that were used for scanning the sample were rather simple which means that this method is computationally light. Even though some of the results were manually picked the uncertainty in the computed parameters was in the millimeter range (2σ), which is acceptable for many applications. This technique could be made automatic by writing a computer algorithm that selects the current manually picked values. This would reduce the subjectivity of the study.

To conclude, the techniques introduced in this study allow true non-contact damage detection of a rectangular notch on a rotating aluminum propeller.

VI. ACKNOWLEDGMENTS

This research did not receive any specific grant from funding agencies in the public, commercial, or not-for-profit sectors.

APPENDIX A: NOTCH DEPTH CALCULATION

To calculate the depth of the notch, one must recur to the dispersion curves for the antisymmetric Lamb wave mode (Fig.8).

One can identify the group velocity of the antisymmetric mode by considering the distance between the excitation and the detection point as well as the time of arrival of the mode (Fig.5). The phase velocity however, has been calculated from the time that it takes a given part of the antisymmetric wave front to interact with the defect, in other words, a part of the wave with a given phase.

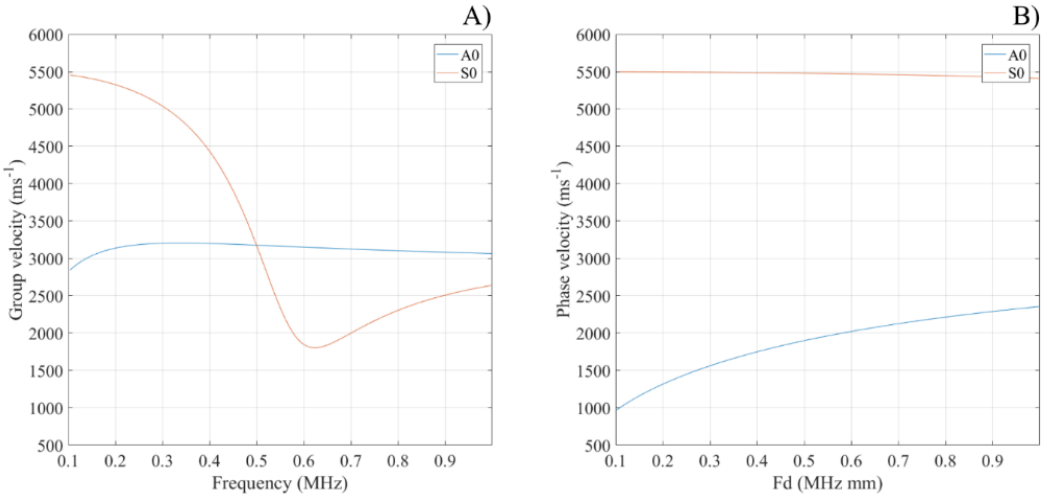

Figure 8. Lamb wave theoretical dispersion curves. A) Group velocity as a function of frequency for a 4 mm thick aluminum plate. B) Phase velocity over frequency times thickness product for an aluminum plate.

The group velocity in the undamaged region of the blade for the antisymmetric mode is $v_g = (3180 \pm 32)\ ms^{-1}$ and the phase velocity in the damaged region $v_2 = (1686 \pm 371)\ ms^{-1}$. From the corresponding dispersion curve (Fig 8A) the central frequency turns out to be f = $(2.09 \pm 0.24)\ 10^5$ Hz . From the phase velocity in the damaged region one can calculate the thickness times frequency product as $Fd = (3.66 \pm 2.08) * 10^5$ Hz mm.

The thickness of the damaged region is then calculated as $T = Fd/f = (1.7 \pm 1.0)$ mm. Since the plate thickness is 4 mm the depth of the notch is $D = (2.3 \pm 1.0)$ mm.

APPENDIX B: UNCERTAINTY CALCULATIONS

All uncertainties reported in this paper have 2σ confidence limits. Since every experiment was repeated three times, the calculated parameters were averaged. Their uncertainty was estimated as:

$$S(x) = \sqrt{S_A(x) + S_B(x)} \qquad \text{(A1)}$$

S(x) is the uncertainty of the x parameter, $S_A(x)$ the standard deviation of the mean, and $S_B(x)$ the empirical uncertainty estimate.

For the linear fit to calculate the group velocity of the A_0 mode (see.Fig.5) the uncertainty in the time of flight was estimated to be $S_B(t) = 0.58$ µs. This uncertainty was derived from the rise time of the A_0 wave front.

$$S_B(v_G) = S(b)/b^2 \qquad \text{(A2)}$$

Here b is the slope of the linear fit to the experimental data whereas $S_B(v_G)$ is the uncertainty in group velocity.

The uncertainty in notch length $S_B(a)$ is estimated as the thickness of the lines in Fig.5 that indicate wave reflection, to be 0.75 mm.

The uncertainty in distance from the center of the sample to the edge of the notch was estimated by propagation of uncertainty.

$$S_B(d) = \sqrt{t^2 S^2(v_g) + v_g^2 S^2(t)} \quad \text{(A3)}$$

Here t is the time of arrival of the reflected A_0 mode and $S(t)$ is its time uncertainty.

The uncertainty in frequency $S_B(f)$ was calculated from the theoretical dispersion curves by subtracting the corresponding frequencies to $v_1 - S(v_1)$ and $v_1 + S(v_1)$. For the notched part of the sample, the uncertainty in the *fd* product $S_B(fd)$ was computed in a similar way. This time by subtracting the corresponding *fd* products for $v_2 - S(v_2)$ and $v_2 + S(v_2)$. Next the uncertainty in notch depth was estimated as:

$$S_B(D) = \sqrt{S^2(fd) + S^2(f)D^2}/f \quad \text{(A4)}$$

From Eq.7 one can use propagation of uncertainties to show that the uncertainty in A_0 group velocity is:

$$S_B(v_2) = \sqrt{\left(\frac{\partial v_2}{\partial R}S(R)\right)^2 + \left(\frac{\partial v_2}{\partial t}S(t)\right)^2 + \left(\frac{\partial v_2}{\partial v_1}S(v_1)\right)^2 + \left(\frac{\partial v_2}{\partial d}S(d)\right)^2} \quad \text{(A5)}$$

$$\frac{\partial v_2}{\partial R} = (t - d/v_1)/(t - (d - R)/v_1)^2 \quad \text{(A6a)}$$

$$\frac{\partial v_2}{\partial t} = -R/(t - (d - R)/v_1) \quad \text{(A6b)}$$

$$\frac{\partial v_2}{\partial v_1} = (R(d - R)/v_1^2)/(t - (d - R)/v_1) \quad \text{(A6c)}$$

$$\frac{\partial v_2}{\partial d} = (R/v_1)/(t - (d - R)/v_1)^2 \quad \text{(A6d)}$$

VII. REFERENCES

[1] FAA, “Aircraft propeller maintenance,” Washington, 2005.

[2] Y.K.An, B.Park and H.Sohn, "Complete noncontact laser ultrasonic imaging for automated crack visualization in a plate," *Smart materials and structures,* vol. 22, pp. 1-10, 2013.

[3] B.Park, H.Sohn, C.Yeum and T.Truong, "Laser ultrasonic imaging and damage detection for a rotating structure," *Structural Health Monitoring,* pp. 494-506, 2013.

[4] R.P.Dalton, P.Cawley and M.J.S.Lowe, "The Potential of Guided Waves for Monitoring Large Areas of Metallic Aircraft Fuselage Structure," *Journal of Nondestructive Evaluation,* vol. 20, no. 1, pp. 29-46, 2001.

[5] "NDT Resource Center," [Online]. Available: https://www.nde-ed.org/EducationResources/CommunityCollege/Other%20Methods/IRT/IR_Intro.php. [Accessed 6 September 2016].

[6] A. International, "Guide to Nondestructive Testing," 2008.

[7] I.Pelivanov, Ł.Ambrozinski, A.Khomenko, E.G.Koricho, G.L.Cloud, M.Haq and M.O'Donnell, "High resolution imaging of impacted CFRP composites with a fiber-optic laser-ultrasound scanner," *Photoacoustics,* pp. 1-10, 2016.

[8] J.M.Bluckley, "An introduction to Eddy Current Testing theory and technology," 2015.

[9] B.Park, H.Sohn, P.Malinowski and W.Ostachowicz, "Delamination localization in wind turbine blades based on adaptive time-of-flight analysis of noncontact laser ultrasonic signals," *Nondestructive Testing and Evaluation,* pp. 1-20, 2016.

[10] C. Escriba, J. Y. Fourniols, M. Lastapis, J. L. Boizard, G. Auriol and S. Andrieu, "New real-time structural health monitoring microsystem for aircraft propeller blades," *IEEE Aerospace and Electronic Systems Magazine,* pp. 29-41, 2012.

[11] H.Lamb, "On Waves in an Elastic Plate," *The Royal Society,* pp. 114-128, 1916.

[12] I.A.Viktorov, Rayleigh and Lamb Waves Physical Theory and Applications, New York: Plenum Press, 1967.

[13] R.Raišutis, E.Jasiūnienė and E. Žukauskas, "Ultrasonic NDT of wind turbine blades using guided waves," *ULTRAGARSAS,* vol. 63, pp. 7-11, 2008.

[14] J.Perdigao and M.Santos, "Leaky Lamb waves for the detection and sizing of defects in bonded aluminium lap joints," *NDT&E International,* vol. 38, pp. 561-568, 2005.

[15] G.Giridhara, V.T.Rathod, S.Naik, D. Mahapatra and S.Gopalakrishnan, "Rapid localization of damage using a circular sensor array and Lamb wave based triangulation," *Elsevier,* vol. 24, pp. 2929-2946, 2010.

[16] E.V.Malyarenko and M.K.Hinders, "Fan beam and double crosshole Lamb wave tomographyf or mapping flaws in aging aircraft structures," *Journal of the Acoustical Society of America,* vol. 108, no. 4, pp. 1631-1639, 2000.

[17] R.E.Green, "Non-contact ultrasonic techniques," *Ultrasonics,* vol. 42, pp. 9-16, 2004.

[18] T.Tanaka and Y.Izawa, "Nondestructive Detection of Small Internal Defects in Carbon Steel by Laser Ultrasonics," *Japan Journal of Applied Physics,* vol. 40, no. 3, pp. 1477-1481, 2001.

[19] M.C.Colin, J.A.López and R.Osguenda, "Identification of Laser-induced Lamb waves," *REVISTA MEXICANA DE FÍSICA,* vol. 53, no. 3, pp. 12-15, 2007.

[20] P.Moilanen, A.Salmi, P.Karppinen, V.Kilappa, J.Timonen, Z.Zhao, R.Myllylä and E.Häeggström, "Photo-Acoustic Phase-Delayed Excitation of Guided Waves in Coated Bone Phantoms," in *ULTSYM,* Prague, 2013.

[21] P.Polynkin, M.Kolesik, J.V.Moloney, G.A.Siviloglou and D.N.Christodoulides, "Curved Plasma Channel Generation Using Ultraintense Airy Beams," *Science,* vol. 324, no. 5924, pp. 229-232, 2009.

[22] J.A.Jakubiec and C.F.Reinhart, "Assessing Disability Glare Potential Due to Reflections from New Constructions: A Case Study Analysis and Recommendations for the Future," The Proceedings of the Transportation Research Board 93rd Annual Meeting, 2014.

[23] S.Krishnaswamy, "Theory and Applications of Laser-Ultrasonic Techniques," in *Ultrasonic Nondestructive Evaluation,* CRC Press, 2003, pp. 435-493.

[24] R.J.Dewhurst and Q. Shan, "Surface-breaking fatigue crack detection using laser ultrasound," *Applied Physics Letters,* vol. 62, no. 21, pp. 2649-2651, 1993.

[25] Y. Nagata, J. Huang, J. D. Achenbach and S. Krishnaswamy, "Lamb wave tomography using laser-based ultrasonics," *Review of Progress in Quantitative Nondestructive Evaluation,* pp. 561-568, 1995.

[26] P.Cawley and D.N.Alleyne, "The Interaction of Lamb Waves with Defects," *IEEE Transactions on Ultrasonics, Ferroelectrics, and Frequency Control,* vol. 39. No 3, pp. 381-397, 1992.

[27] J.P.Jiao, W.H.Liu, C.F.He, B.Wu and J. Zhang, "Nonlinear Acoustic Interaction of Contact Interfaces," *Experimental Mechanics,* vol. 54, pp. 63-69, 2014.

[28] R.S.Panda, P.Rajagopal and K.Balasubramaniam, "Characterization of delamination-type damages in composite laminates using guided wave visualization and air-coupled ultrasound," *Structural Helath Monitoring,* pp. 1-11, 2016.

[29] F.Uzun and A. N. Bilge, "Non-Destructive Investigation of Bulk Residual Stress in Automobile Brake Pads with its Service Life," *Journal for Foundations and Applications of Physics,* vol. 3, no. 2, pp. 94-102, 2016.

[30] M. Koshiba, S. Karakida and M.Suzuk, "Finite-Element Analysis of Lamb Wave Scattering in an Elastic Plate Waveguide," *IEEE transactions on sonics and ultrasonics,* Vols. SU-31, NO 1, pp. 18-24, 1984.

[31] N.Cite, F. Chati, D. Décultot, F. Léon and G. Mazea, "Acoustic scattering from a finite plate: Generation of guided Lamb waves S0, A0 and A," *Accoustical Society of America,* vol. 131, no. 6, pp. 4233-4242, 2012.

[32] M.Noroy, D.Royer and M.Fink, "The laser-generated ultrasonic phased array : Analysis and experiments," *Acoustical Society of America,* vol. 94, no. 4, pp. 1934-1943, 1993.

[33] C.Prada, O.Balogun and T.W.Murray, "Laser-based ultrasonic generation and detection of zero-group velocity Lamb waves in thin plates," *Applied Physics Letters,* vol. 87, pp. 1-3, 2005.

[34] P.Karppinen, A.Salmi, P.Moilanen, T.Karppinen, Z.Zhao, R.Myllylä, J.Timonen and E.Hæggström, "Phase-delayed laser diode array allows ultrasonic guided wave mode selection and tuning," *Journal of Applied Physics,* vol. 113, pp. 1-5, 2013.

[35] B.J.Fryer and M.E.Shaheen,
"Femtosecond laser ablation of brass: A study of surface morphology and ablation rate," *Laser and Particle Beams,* pp. 473-478, 2012.